Chemical and Process Engineering: New Frontiers, 2024, 45(4), e77
DOI: 10.24425/cpe.2024.149472

# Chemical engineering aspects in the design and construction of a new type of multimaterial 3D printer using photopolymerization and electrodeposition processes

Maciej Pilch[1*], Dawid Kiesiewicz[1,2], Bartosz Oksiuta[2], Joanna Ortyl[2]

[1] Cracow University of Technology, Faculty of Civil Engineering, Wind Engineering Laboratory, Warszawska 24, 31-155 Cracow, Poland
[2] Cracow University of Technology, Faculty of Chemical Engineering and Technology, Department of Biotechnology and Physical Chemistry, Warszawska 24, 31-155 Cracow, Poland

*** Corresponding author, e-mail:** maciej.pilch@pk.edu.pl

Presented at
4rd Seminar on Practical Aspects of Chemical Engineering PAIC 2024, 16–17 May 2024, Zaniemyśl, Poland. Guest Editors: Andżelika Krupińska and Sylwia Włodarczak.

**Article info:**
Received: 21 July 2024
Revised: 03 September 2024
Accepted: 14 November 2024

**Abstract**
3D printing has recently been experiencing a period of extremely rapid development. This is due to the fact that researchers as well as the industry recognize the many advantages of 3D printing. The dynamic development of this field brings about the advancement of new technologies, leading to the search for new photocurable resin formulations that enable efficient 3D printing in various environments. The development of an appropriate photocurable resin for 3D printing in the aqueous environment of electroplating baths is a crucial aspect in designing new devices for multi-material 3D printing that utilize coupled processes of electrodeposition and photopolymerization. Therefore, this article analyzes the effect of different environments on the kinetics of the photopolymerization process of photo-curable compositions dedicated to 3D printing. The study was carried out in four different environments: argon, water, saturated copper (II) sulfate solution and saturated copper (II) sulfate solution acidified with monomolar sulfuric (VI) acid. The work used techniques such as Fluorescent Probe Technique, photorheology, rheology and Raman spectroscopy to investigate the course of the photopolymerization process. The results of the experiments showed that the environment has a significant effect on the degree of conversion of monomers and on the rate of the photopolymerization process itself.

**Keywords**
3D printing, photopolymerization, photorheology, Raman spectroscopy, multimaterial 3D printer

## 1. INTRODUCTION

The development of Industry 4.0 is currently one of the most rapidly growing industries, which integrates digital and physical systems and has a significant impact on the speed, efficiency and course of technological processes. Industry 4.0 signifies a transformation towards intelligent manufacturing, where machines communicate and work closely together, exemplifying a significant increase in productivity and reduction of production waste, energy consumption and costs (Jandyal et al., 2022; Olsen and Tomlin, 2019; Peruzzini et al., 2020).

The growing demand for state-of-the-art solutions is making additive prototyping technologies increasingly popular and thus intensely sought after (Pagac et al., 2021). They are indispensable tools for creating prototypes and demonstration models that largely reflect the features of the final product, such as physical properties, ergonomics of use or aesthetics, among others. Some of the fastest, most accurate, efficient and widely available methods used to prototype such objects are 3D printing technologies related to photopolymerization processes (Praveena et al., 2022; Shahrubudin et al., 2019).

The photopolymerization process involves curing photocurable resins under UV light, enabling the rapid creation of precise, durable and highly complex structures (Topa-Skwarczyńska et al., 2022). Common 3D printing techniques using photopolymerization are SLA (stereolithography) , DLP (digital light processing) and CLIP (continuous manufacturing on a liquid surface) (Praveena et al., 2022).

The SLA method, is the oldest 3D printing technology using photo-curable materials. Its main advantages are high process stability and high availability of equipment, while the disadvantages include low productivity. It uses a UV laser to draw a cross section layer by layer on a structural plate moving in small increments (Khadilkar et al., 2019). The technology is used in dentistry, toy manufacturing, automotive and aerospace (Ahn et al., 2020; Bagheri and Jin, 2019; Gibson et al., 2010; Quan et al., 2020; Topa-Skwarczyńska et al., 2022).

In contrast, DLP 3D printing technology uses a digital projector to expose and cure layers of liquid photopolymer resin. DLP technology is known for its fast curing process and high precision printing, due to the simultaneous curing of the entire resin layer (Kowsari et al., 2018). The method is used in many fields, including dentistry, jewelry and electronic components (Ahn et al., 2020; Bagheri and Jin, 2019; Gibson et al., 2010; Quan et al., 2020; Topa-Skwarczyńska et al., 2022).

Continuous Liquid Interface Production (CLIP) 3D printing technology is a relatively new method that is considered

revolutionary (Huang et al., 2022). It uses UV light and an oxygen permeable membrane, which prevents resin from adhering to the screen, to cure liquid photopolymer resin continuously. It features a very fast printing process and high precision (Ahn et al., 2020; Bagheri and Jin, 2019; Quan et al., 2020; Topa-Skwarczyńska et al., 2022).

Another 3D printing technique using photocurable resins differs somewhat from the others and is more similar to the FDM (Fused Deposition Modeling) technique used for 3D printing with filaments. It can be called the resin extrusion technique. In this technique, photocurable resin is extruded through a special nozzle onto the worktable and then cured with UV light. The mechanical construction of these types of printers is very similar to FDM printers. The advantage of this 3D printing technique is primarily the ability to easily print with resins doped with a variety of materials that would not be possible to print using standard DLP or SLA techniques. Unfortunately, this technique is characterized by lower printing accuracy compared to SLA or DLP techniques (Asif et al., 2017; 2018).

The second very important group of materials used in 3D printing, besides plastics, are metals. Metals are primarily characterized by higher thermal resistance compared to plastics, as well as high mechanical strength and good tribological properties. 3D printing with metal is significantly more demanding than that with plastics. In practice, industrial 3D metal printers mainly use the process of sintering metal powders with a high-energy beam, such as a laser beam, occurring at very high temperatures of several thousand degrees Celsius.

The first group of techniques, where metal powder is spread as a uniform layer on the worktable and then selectively sintered with a high-energy beam, includes SLM (Selective Laser Melting) and EBM (Electron Beam Melting) techniques. SLM printers use selective laser melting technology for metal powders using a high-power laser beam. In EBM printers, an electron beam is used instead of a laser beam.

The second group of methods includes LMD (Laser Material Deposition) and EBAM (Electron Beam Additive Manufacturing) techniques, where a single head simultaneously doses and melts the metal raw material (powder or wire). It can be said that LMD technology is equivalent to the SLM technique. In this case, the metal powder is precisely dosed using a movable nozzle and melted with a laser. In the EBAM technique, instead of metal powder, a metal wire is used, which is fed from an appropriate head and melted with a laser.

Another group of methods includes Binder Jetting and related techniques, often using photocurable polymer binders to initially bind metal powders together during the 3D printing process, after which the printed components are sintered in high-temperature furnaces to achieve a solid metal structure (Yakout et al., 2018; Yang et al., 2017)

The common feature of all these methods is the use of high temperature to create a solid metal structure during 3D printing or post-processing.

A completely different technique for producing 3D metal components with complex spatial geometry is the 3D printing technique using metal electrodeposition, developed in recent years. In this method, successive layers of metal are produced by the reduction of metal ions contained in the solution on a conductive surface (e.g., metal). Many scientists worldwide are working on the development of this technology due to its high implementation potential. These solutions are currently detailed in the literature (Chen et al., 2017), although in practice they are rarely used on a larger scale due to the significantly limited printing speed with this technique. However, the primary advantage of this technique is the ability to additively produce layers of solid metal at room temperature. It is the first existing 3D printing technique in the world that allows this. Consequently, it becomes possible to combine 3D metal printing with other processes that require being conducted at not too high temperatures, such as 3D printing with plastics. This issue is currently of interest to many scientists and companies in the 3D printing industry.

Work is underway to develop a hybrid technology, allowing 3D printing of metal-polymer hybrid parts (Ambrosi et al., 2020). Such an approach can combine the advantages of both materials: strength, durability and thermal resistance of metals with the flexibility, low density and ease of polymer additive manufacturing. Hybrid metal-polymer components can be up to 40% lighter than solid metal parts while maintaining very similar mechanical strength. This creates the potential for widespread application of this technology in industries such as marine, automotive, aviation and aerospace, where the weight-to-strength ratio of used components (transport machinery parts) is crucial. Reports on attempts to develop such 3D printing technology using coupled electrodeposition and photopolymerization processes already exist in the literature (Ambrosi et al., 2020). So far, however, it has not been possible to develop a full-fledged 3D printer enabling 3D printing of functional hybrid metal-polymer details with dimensions corresponding to the standard working areas of 3D printers for plastics (approx. 20 cm $\times$ 20 cm $\times$ 20 cm). Currently, research and development efforts are focused on creating a functional device for multi-material 3D printing that allows for the printing of functional hybrid metal-polymer 3D details, where some parts of a given detail are made of metal and others of polymer. Since, in such 3D printing device, the metal parts of a given component are to be produced via metal electrodeposition, which is usually conducted from aqueous electroplating solutions, it is technically advantageous for the polymer part printing process to also occur in the aqueous electroplating bath environment. The use of electrodeposition in 3D printing technology for hybrid parts is essential, as it is one of the few processes that enables additive manufacturing of solid metal structures at room temperature. To enable the 3D printing of polymer parts using photopolymerization in an aqueous electroplating solutions environment, the chosen 3D printing technique involves the extrusion of a photocurable resin in the aqueous electroplating

bath through a suitable nozzle, followed by curing with UV light. The key issue in this regard is the formulation of an appropriate photocurable resin, which should have sufficiently high viscosity to maintain coherence in the aqueous electroplating bath environment during extrusion through the nozzle and a highly efficient photoinitiating system capable of effectively initiating the photopolymerization process even after UV light passes through the layer of electroplating solution, which can partially absorb and scatter UV light. Therefore, this article analyzes the effect of different environments on the kinetics of the photopolymerization process of photo-curable compositions dedicated to 3D printing (Chen et al., 2017).

## 2. EXPERIMENTAL PART

This article presents the effects of the environment of argon, water, saturated $CuSO_4$ solution and saturated $CuSO_4$ solution acidified with monomolar $H_2SO_4$ on the course of photopolymerization reaction of photocurable resins dedicated to 3D printing in aqueous electrolyte solutions. Copper sulfate solution was chosen as the environment for studying the photopolymerization rate due to the fact that solutions of this salt are commonly used as the basis for electroplating baths employed in copper electrodeposition. Copper electrodeposition is a model process for metal electrodeposition from aqueous solutions and is therefore currently being used in research on multi-material 3D printers that utilize electrodeposition for 3D printing of metal parts.

### 2.1. Materials

The monomers used were EBECRYL 1291 (Allinex), EBECRYL 4740 (Allinex), EBECRYL 4858 (Allinex) and the oligomer EBECRYL 285 (Allinex). Diphenyl(2,4,6-trimethylbenzoyl)phosphine oxide (TPO) (Allinex) was used as the initiator. For measurements using the FPT technique, 2,3,6,7-Tetrahydro-9-methyl-1H,5H-quinolizino(9,1-gh)coumarin (Coumarin 102, Sigma Aldrich) was used as a fluorescent probe. (Fig. 1)

### 2.2. Methods

#### 2.2.1. Raman spectroscopy

The first group of studies on the kinetics of photopolymerization reactions in aqueous media were performed using Raman spectroscopy (Eq. (1)). Commercially available resins from the EBECRYL®series were used in this study. Such resins are characterized by viscosity in the range of 1900–23000 mPa·s (parameters given by the manufacturer), which allows their use in extrusion 3D printing and also ensures sufficient preservation of composition consistency in aqueous environments, which translates into minimizing the adverse effects of leaching, but still retaining properties that allow free extrusion through nozzles, which are typically used in commercial extrusion 3D printers. In addition, such compositions have a density higher than that of water, thus excluding the adverse effects of liquid floatation during printing in aqueous environments (Duty et al., 2018; Lee et al., 2017; Meenakshisundaram et al., 2024; Ngo et al., 2018; Randhawa et al., 2023; Rau et al., 2021; Zheng et al., 2018). Diphenyl(2,4,6-trimethylbenzoyl)phosphine oxide (TPO) (1% by weight), which is very efficient and widely used in industry, was added to the formulation as a photoinitiator. This initiator photodissociates when exposed to light in the visible range and thus effectively initiates the photopolymerization process (Leprince et al., 2011; de Oliveira et al., 2016; Topa-Skwarczyńska et al., 2022). The formulations prepared in this way were irradiated with UV light with maximum emission at 365 nm wavelength to initiate the photopolymerization process and were subjected to spectroscopic analysis to determine

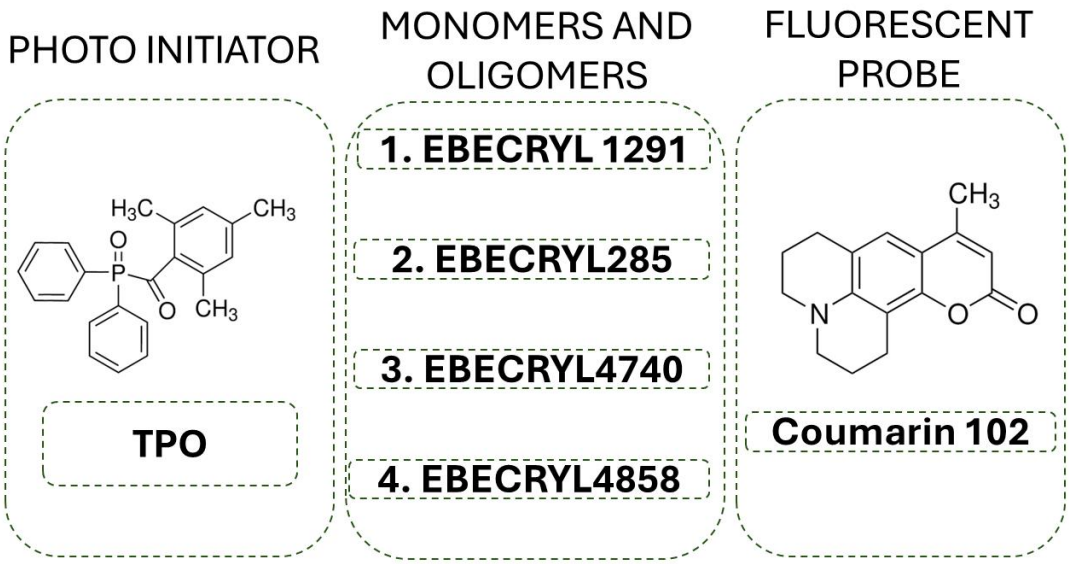


Figure 1. Structures of initiator used for photopolymerisation processes, fluorescent probes and names of used monomers and oligomers.

the effect of different environments on the characteristics of the photopolymerization process and the degree of conversion. Samples tested in an argon environment were used as a control, while it should be noted that samples were not tested in a $CuSO_4$ solution environment due to the absorption of the laser's IR radiation by the colored copper(II) sulfate solution.

The kinetics of photopolymerization was studied by real-time Raman spectroscopy, using an Anton Paar Cora 5001 spectrometer with a Fiber package and an attachment that allows measurements made in-house (Fig. 2).

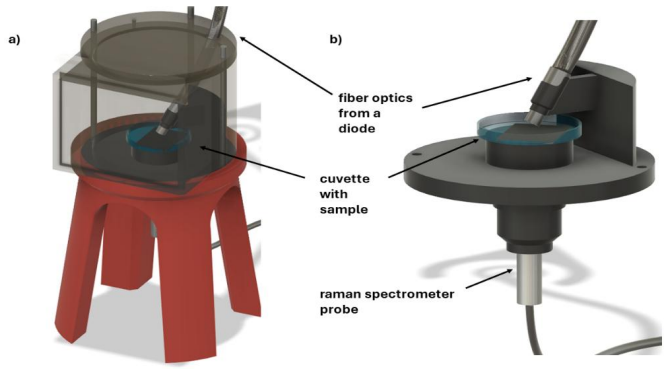


Figure 2. Visualization of the author's conversion measurement attachment using Raman spectroscopy made by 3D printing. The visualization was made in Fusion360 software (Autodesk).

The measurement consisted of placing a few drops of the appropriate composition in a ring with an inner diameter of 5 mm and a thickness of 1mm, pasted on polypropylene film. The sample prepared in this way was then placed in a cuvette, which was completed along the wall using a pipette to minimize the effect of sample blurring. The sample thus prepared, together with the cuvette, was placed in the measuring chamber of the spectrometer. Measurements of photopolymerization kinetics were carried out with a polymerization time of 2000 seconds. The experiments were conducted in a dark room where the only light source was the diode used in the experiment. The light source in the real-time experiment for the Raman method was an M365L2 diode (Thorlabs Inc., Newton, NJ, USA) with a power of 15 mW/cm$^2$ (this value was controlled with PM160 - Si Sensor Power (Thorlabs Inc.), powered by a regulated DC2200 power supply (Thorlabs Inc., Newton, NJ, USA). The UV-LED was turned on immediately after the first scan of the spectrometer. The distance between the light source and the samples was 15 mm.

Since the decrease in peak area absorption is directly proportional to the number of polymerized groups, the degree of functional group conversion was calculated by measuring the peak area at each reaction time, using the equation:

$$C_{\text{Raman}}\,[\%] = \left(1 - \frac{A_{\text{After}}}{A_{\text{Before}}}\right) \cdot 100\% \qquad (1)$$

where $A_{\text{Before}}$ is the area of the band specific to the monomer used and the type of photopolymerization before the photopolymerization process, while $A_{\text{After}}$ is the area of the same band but after the polymerization process.

The monitored band is 1634 cm$^{-1}$ which is responsible for the double bonds in the monomer and which disappear in proportion to the progress of the photopolymerization process.

### 2.2.2. Fluorescent probe technique

In order to obtain more data on the polymerization kinetics of the photo-curable compositions, such as the induction time or the rate of the initial polymerization reaction, the FPT (Fluorescent Probe Technique) was used, which is well suited for studying such parameters (Kamińska et al., 2015; Ortyl et al., 2012; Sawicz-Kryniger et al., 2022). As a fluorescent probe, 2,3,6,7-Tetrahydro-9-methyl-1H,5H-quinolizino(9,1-gh)coumarin (Coumarin 102) was chosen, which absorbs well the UV light with a wavelength of 365 nm, with which the samples were irradiated (Kamińska et al., 2016). The tests were performed on samples consisting of the following monomers: EBECRYL 285, EBECRYL 1291, EBECRYL 4740, EBECRYL 4858 with the addition of a 1% wt. TPO initiator and the addition of 0.1% wt. Coumarin 102 as the fluorescent probe. The samples were irradiated with UV-LED diode with a maximum emission wavelength of light at 365 nm, with an intensity equal to 15 mW/cm$^2$. The tests were carried out in the following environments: distilled water, saturated aqueous copper(II) sulfate solution and saturated aqueous copper(II) sulfate solution acidified with monomolar $H_2SO_4$.

The photopolymerization monitoring system (Fig. 3) consisted of a specially designed sample chamber with a head, where an optical fiber of a miniature CCD spectrometer (EPP2000C, StellarNet Inc., USA) connected to a microcomputer for data acquisition, (UVTOP315-BL-TO39, Roithner LaserTechnik GmbH, Austria) and a UV LED emitting light with a wavelength of $\lambda_{\text{max}} = 365$ nm was placed. The UV LED was

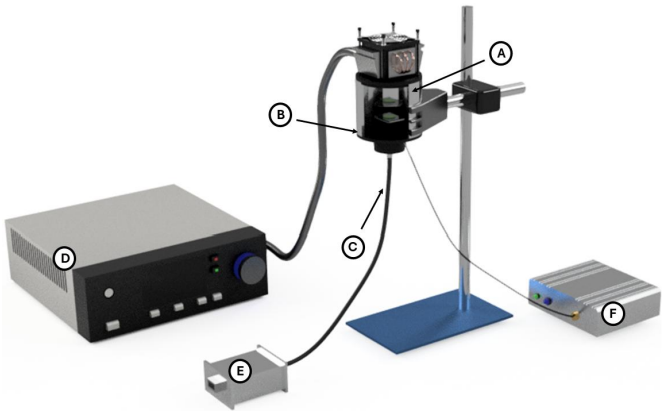


Figure 3. 3D visualization (made in Autodesk Fusion360 software) of the FPT measurement station with a cross-section in the measurement chamber. A – Peltier module with heat sink, B – tested sample, C – diode, D – thermostat, E – diode power supply, F – light fiber.

powered with a constant current from a suitable stabilized DC source, giving light with an intensity of 15 mW/cm$^2$, a parameter that was controlled using PM160 – Si Sensor Power (Thorlabs Inc.). This is a version of a measurement system used previously (Kamińska et al., 2015). The sensor head and the top and bottom covers of the sample chamber were made of round aluminum blocks.

Sample preparation for measurements consisted of injecting the composition into a pre-prepared ring with a thickness of 0.1 mm and an inner diameter of 12 mm which was glued onto a microscope slide. The tests were carried out for each sample in four environments: argon, distilled water, saturated copper sulfate solution and saturated copper sulfate solution with the addition of sulfuric acid (IV) at a concentration of 1 mol/dm$^3$. The prepared samples were placed in a pan which was then filled with the appropriate solution along the wall so as to reduce the effect of sample smearing. The amount of solution in the pan was chosen so that there would be a 5 mm thick layer of liquid over the sample. For measurements in an argon environment, the chamber was purged with the gas for 2 minutes. Before the measurements of all samples, the chamber was thermostated until a stable temperature of 25 °C was reached.

The degree of polymerization progress was determined by the ratio of fluorescence intensity (R). The R parameter was defined as the ratio of fluorescence intensity at the shorter wavelength ($\lambda_1$) to that at the longer wavelength ($\lambda_2$). The wavelengths $\lambda_1$ and $\lambda_2$ were selected individually for the probe to correspond to half the height of the fluorescence spectrum before polymerization (Szymaszek et al., 2023). Initial R value was 1 and increased as polymerization progressed. Measurements were taken every 3 seconds during the first 150 scans to precisely record the changes occurring during photopolymerization, and then the time interval was increased to 32 seconds for the next 100 scans to capture the plateau in kinetic profiles.

#### 2.2.3. Photo-rheological tests

The next group of tests includes rheological and photo-rheological tests of the analyzed photocurable resins. In view of the potential application of the studied formulations in 3D printing, studies were carried out to determine the exact rheological characteristics of the prepared resins, including the gel point. These studies allowed us to understand the dynamic rheological changes that occur during the photopolymerization process, which is important for 3D printing parameters. Thanks to photorheology, it is possible to monitor changes in viscosity and rheological modules in real time, which makes it possible to precisely determine when a material transitions from a liquid to a solid state (Szymaszek et al., 2023). The samples consisted of monomers: EBECRYL 285 (E285), EBECRYL 1291 (E1291), EBECRYL 4740 (E4740), EBECRYL 4858 (E4858) in the presence of TPO (1% by weight) initiator. The tests were carried out using a UV-LED with maximum emission at 365 nm wavelength on an Anton Paar Physica MCR 302 rheometer using a special attachment that allows photorheological measurements. In addition, to complete the characterization of the tested formulations, rheological tests of liquid uncured resins were carried out. The tests were carried out at 25 °C, using a Physica MCR 302 rheometer from Anton Paar. The samples consisted of monomers: EBECRYL 285 (E285), EBECRYL 1291 (E1291), EBECRYL 4740 (E4740), EBECRYL 4858 (E4858) in the presence of TPO (1% by weight) initiator.

Photorheological and rheological measurements were carried out to determine the characteristics of the tested formulations such as the gel point and viscosity determination. The gel point was determined as the intersection point of storage and loss moduli.

Rheological behavior was studied using a Physica MCR 302 rheometer (Anton Paar) equipped with 20 mm diameter parallel plate geometries. The bottom geometry was made of quartz, which allowed exposure and in-situ photo-curing. The experiments used a 365 nm diode (Thorlabs Inc.) with a light intensity of 30 mW/cm$^2$, and the value was controlled with PM160 – Si Sensor Power (Thorlabs Inc.).

Photorheological experiments were carried out with a nominal distance between the top and bottom geometries of the system (slit) of 0.2 mm, using 20 mm diameter spindles, and the process was carried out under isothermal conditions (at 25 °C). A 60-second dark period was used to stabilize the sample, after which the light was turned on.

Studies of the rheological properties of the photo-curable compositions were also performed under isothermal conditions (temperature of 25 °C) with a zero gap setting of 0.2 mm on a 25 mm diameter spindle. The tests began by placing the sample on the base of the rheometer and setting the zero gap. After the spindle reached the preset distance from the base, the excess composition was collected and then the measurement began. The measurement was carried out with a variable spindle speed (shear rate) ranging from 1/s to 100/s over a period of 100 seconds.

## 3. RESULTS AND DISCUSSION

This chapter presents the kinetic profiles of the photopolymerization reactions of the analyzed acrylate and acrylate-urethane monomers in various environments, determined using Raman spectroscopy, Fluorescent Probe Technology, and photorheological tests. The standard rheological characteristics of the resins used, as well as observations and conclusions regarding the progress of the photopolymerization reactions in various environments, are also presented. Additionally, the applicability of the analyzed photocurable resins for 3D printing in aqueous electrolyte solutions is discussed in this chapter.

### 3.1. Raman spectroscopy

The kinetic profiles in the form of the change in monomer conversion degree during the photopolymerization process, determined using Raman spectroscopy, are presented in Figure 1. In the case of compositions with the monomer EBECRYL 1291 (E1291) and EBECRYL 4740 (E4740), a significant scatter of measurement points can be observed for tests in aqueous environments. This may be due to the movements of the liquid in which the sample was immersed. The conversion results for compositions in aqueous environments were lower than in the argon environment. This is because the light source was placed above the sample at a 60° angle, causing the light beam to first pass through the water surface before it could illuminate the photocurable composition. The conversion values of photocurable compositions mainly depend on the number of functional groups capable of forming bonds. For compositions consisting of acrylate monomers, conversion values often hover around 60%. The sample consisting of the monomer EBECRYL 1291 (E1291) contains a hexafunctional urethane acrylate. Based on the conversion results, it can be assumed that only three out of the six functional groups participate in the polymerization process before the molecule becomes completely rigid (Fig. 4, Tab. 1).

Analyzing the obtained conversion values in different environments, it can be concluded that all the studied compositions may be suitable for use as material for 3D printing hybrid parts in aqueous environments. During 3D printing with such resins in an aqueous environment, a much stronger UV light source must be used to ensure a sufficiently rapid photopolymerization process. An important aspect is that the resin retains its shape after the printing process. Samples were subjected to organoleptic analysis by compressing them.

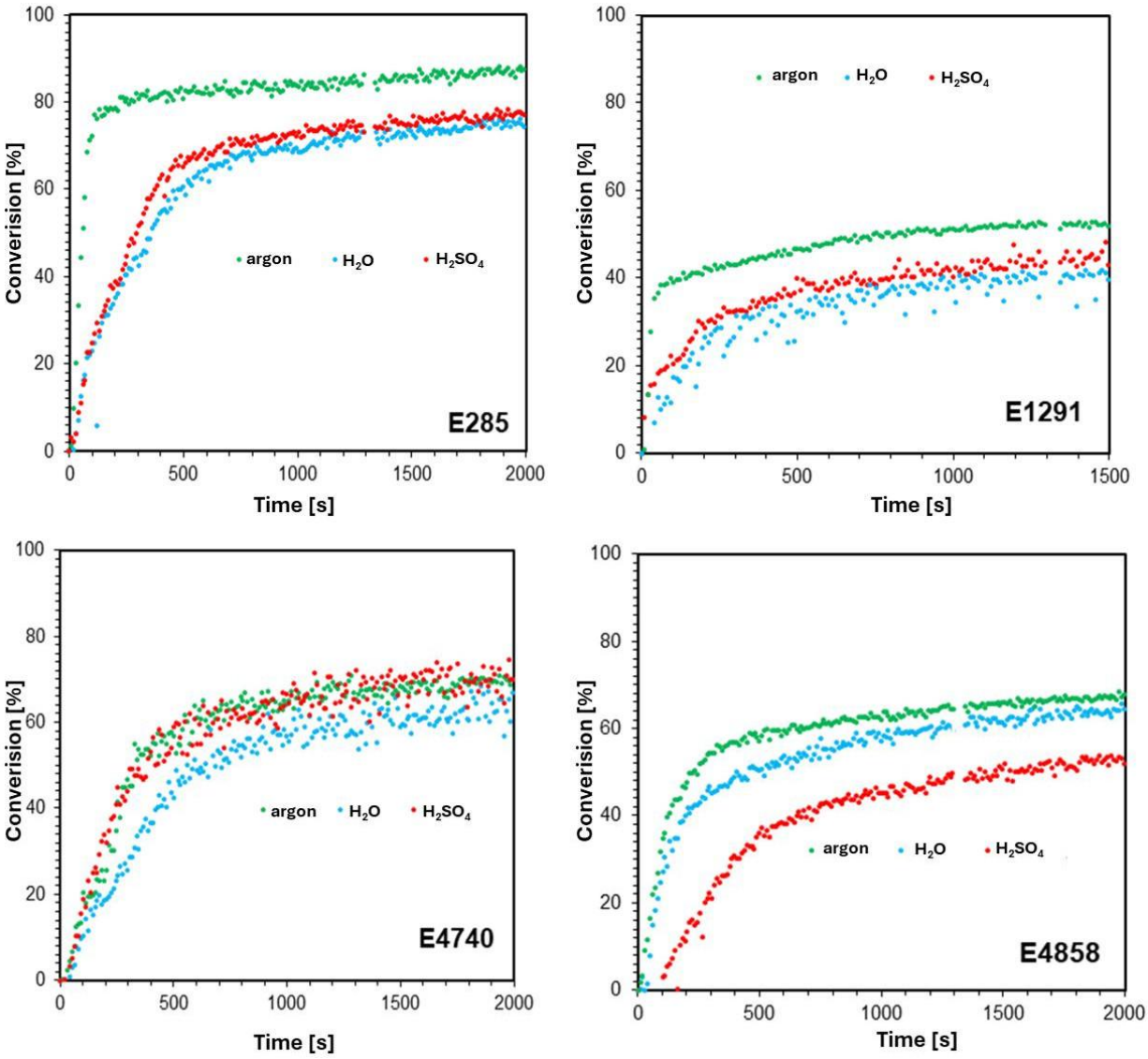


Figure 4. Photopolymerization kinetic profiles for compositions based on monomers: EBECRYL 285 (E285), EBECRYL 1291 (E1291), EBECRYL 4740 (E4740), EBECRYL 4858 (E4858) in the presence of. TPO (1% w/w) initiator after LED irradiation with maximum emission at 365 nm (15 mW/cm$^2$) in various environments.

Table 1. Summary of the conversion of functional groups in photopolymerization processes after LED irradiation with maximum emission at 365 nm (15 mW/cm$^2$).

| Sample name | Environment | Conversion [%] | Sample name | Environment | Conversion [%] |
|---|---|---|---|---|---|
| E285 | Argon | 87 | E4740 | Argon | 71 |
| | Water | 75 | | Water | 64 |
| | $H_2SO_4$ | 78 | | $H_2SO_4$ | 70 |
| E1291 | Argon | 52 | E4858 | Argon | 68 |
| | Water | 42 | | Water | 64 |
| | $H_2SO_4$ | 45 | | $H_2SO_4$ | 54 |

All samples behaved like uniform solids, indicating that they have the ability to retain their shape despite not achieving a complete degree of conversion.

## 3.2. Fluorescent Probe Technique

The most important parameters that can be determined from the kinetic polymerization profiles obtained using FPT (Fluorescent Probe Technology) are the induction time ($t_{ind}$) and the initial polymerization rate $(dR/dt)_0$. In most cases, the induction time of photocurable compositions is lowest in an argon environment, followed by an aqueous environment, then in a saturated copper(II) sulfate solution and highest in a saturated copper(II) sulfate solution acidified with monomolar $H_2SO_4$. This is because the argon environment eliminates the phenomenon of oxygen inhibition. In the aqueous environment, oxygen is dissolved in the water. The saturated copper(II) sulfate solution contains copper ions that strongly capture oxygen from the air, and the addition of sulfuric acid ensures that all the copper in the solution is in ionic form. Regarding the initial polymerization rate, it is higher in aqueous environments than in the argon environment. This is likely due to two factors. One factor is that the ultraviolet light source is positioned perpendicularly to the sample from the bottom, so in the argon environment, the beam passes through the sample and stops at the chamber cover, while in aqueous environments, the light beam is additionally reflected back onto the composition upon encountering the surface of the solution. Another factor could be the change in sample thickness during polymerization. The ring in which the sample is placed has a diameter of 12 mm, while the aperture through which the light beam passes has a diameter of 5 mm, so not the entire composition is illuminated during the measurement. During illumination, the composition outside the perimeter through which the light beam passes flows into the area where photopolymerization occurs, caused by polymerization shrinkage. In measurements conducted in an aqueous environment, there are hindrances to the migration of the composition caused by the resistance of the solution surrounding the sample, meaning that fresh, unpolymerized portions of the composition do not flow into the photopolymerization area as they do in the argon environment. The initial polymerization rate, however, does not significantly differ depending on the polymerization environment (Fig. 5, Tab. 2).

Analyzing the obtained results, it can be hypothesized that there is no dependence between the initial photopolymerization rate of the analyzed monomers and their environment. However, there is a dependence between the induction time of photopolymerization of the analyzed monomers and their

Table 2. Summary of monitoring photopolymerization processes using FPT technique after LED irradiation with maximum emission at 365 nm wavelength (15 mW/cm$^2$), where: $t_{ind}$ [s] – induction time; $(dR/dt)_0$ – the initial rate of the polymerization process.

| Sample name | Environment | $(dR/dt)_0$ | $t_{ind}$ [s] | Sample name | Environment | $(dR/dt)_0$ | $t_{ind}$[s] |
|---|---|---|---|---|---|---|---|
| E285 | Argon | 0.00404 | 13.57 | E4740 | Argon | 0.00781 | 11.29 |
| | Water | 0.00508 | 16.87 | | Water | 0.00662 | 14.79 |
| | $CuSO_4$ | 0.00620 | 18.56 | | $CuSO_4$ | 0.00913 | 15.50 |
| | $CuSO_4$-$H_2SO_4$ | 0.00457 | 18.60 | | $CuSO_4$-$H_2SO_4$ | 0.00968 | 16.22 |
| E1291 | Argon | 0.00103 | 21.62 | E4858 | Argon | 0.00791 | 10.40 |
| | Water | 0.00185 | 21.60 | | Water | 0.00764 | 12.78 |
| | $CuSO_4$ | 0.00136 | 21.60 | | $CuSO_4$ | 0.00785 | 14.85 |
| | $CuSO_4$-$H_2SO_4$ | 0.00168 | 22.89 | | $CuSO_4$-$H_2SO_4$ | 0.00750 | 18.83 |

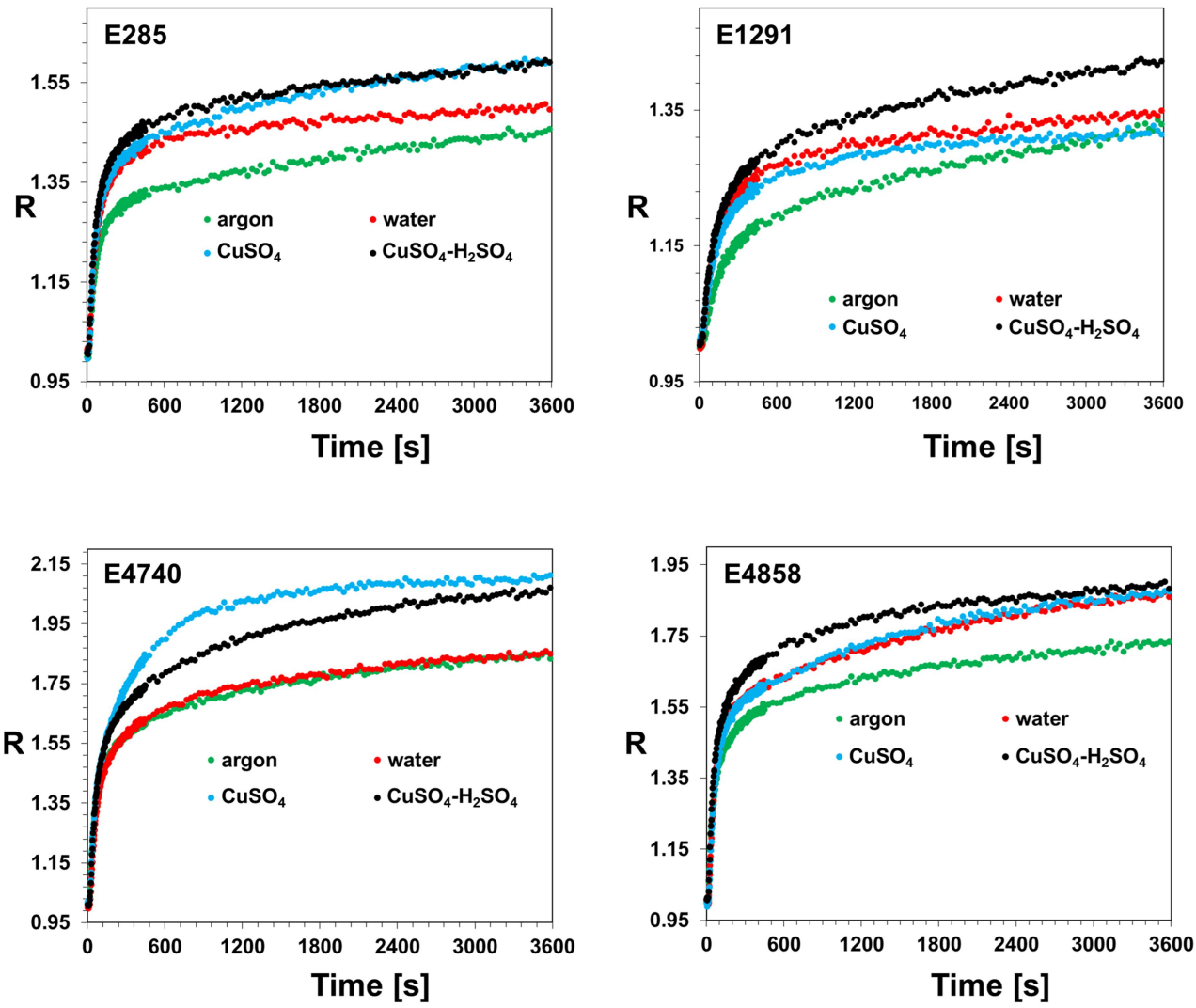


Figure 5. Photopolymerization monitoring for monomer-based compositions: EBECRYL 285 (E285), EBECRYL 1291 (E1291), EBECRYL 4740 (E4740), EBECRYL 4858 (E4858) in the presence of. TPO (1% w/w) initiator using Coumarine 1 fluorescent probe (0.1% w/w) after UV-LED irradiation with maximum emission at 365 nm and light intensity of 15 mW/cm$^2$.

environment. Based on the literature, we can conclude that this dependence is mainly due to the different solubility of atmospheric oxygen, as well as the presence of copper ions in the solution. Based on the FPT measurements, it can be concluded that, in most cases, the induction time of photocurable compositions is shortest in an argon environment, followed by an aqueous environment, then in a saturated copper(II) sulfate solution and is longest in a saturated copper(II) sulfate solution with one molar sulfuric acid. This is because the argon environment eliminates the phenomenon of oxygen inhibition. In the aqueous environment, oxygen is dissolved in the water. The presence of oxygen in the sample's surroundings causes the quenching of free radicals, which contributes to slowing down the photopolymerization process (increasing the induction time of photopolymerization) (Simič et al., 2021). In the copper (II) sulfate solution environment, in addition to the oxygen inhibition phenomenon resulting from the presence of dissolved oxygen, we can also observe inhibition and chain termination caused by copper ions (Abramov et al., 1989). The addition of sulfuric acid ensures that all the copper in the solution is in the ionic form, which further intensifies the inhibition and chain termination effects caused by copper ions.

## 3.3. Photo-rheological tests

Based on photorheological measurements for each of the analyzed photocurable compositions, the gel point and polymerization shrinkage were determined. The gel point indicates the degree of conversion of the monomer's functional groups, corresponding to the appearance of molecules in the system with a polymerization degree significantly higher than that of the remaining molecules in the system (forming a so-called gel). These measurements can determine which composition polymerizes the fastest under given conditions. The value of polymerization shrinkage is very important in the 3D print-

ing process with photocurable resins, especially in the case of printing metal-plastic connections. If there is excessive polymerization shrinkage during the polymerization of the composition on the metal surface, structural defects may form, significantly weakening the metal-plastic bond (Fig. 6, Tab. 3).

Analyzing the presented measurement results, it can be concluded that the gel point is reached latest by the E1291 composition, while the E4740 composition reaches it the fastest. The polymerization shrinkage of the analyzed compositions does not reach high values (the highest shrinkage is 1.5% for the E4858 composition), so it can be assumed that its impact on the formation of structural defects in the printed parts using analyzed resins is negligibly small.

## 4. SUMMARY AND CONCLUSIONS

This paper presents innovative research on the photopolymerization of photocurable resins in various environments, including an aqueous copper sulfate solution. Additionally, rheological studies of these photocurable resins in these environments were conducted, focusing on evaluating the potential use of these resins for 3D printing in aqueous electrolyte solutions (electroplating baths).

These studies have established that there are photocurable resins capable of maintaining integrity in aqueous electrolyte solutions while demonstrating high efficiency in photoinitiated polymerization. This finding supports the potential use of

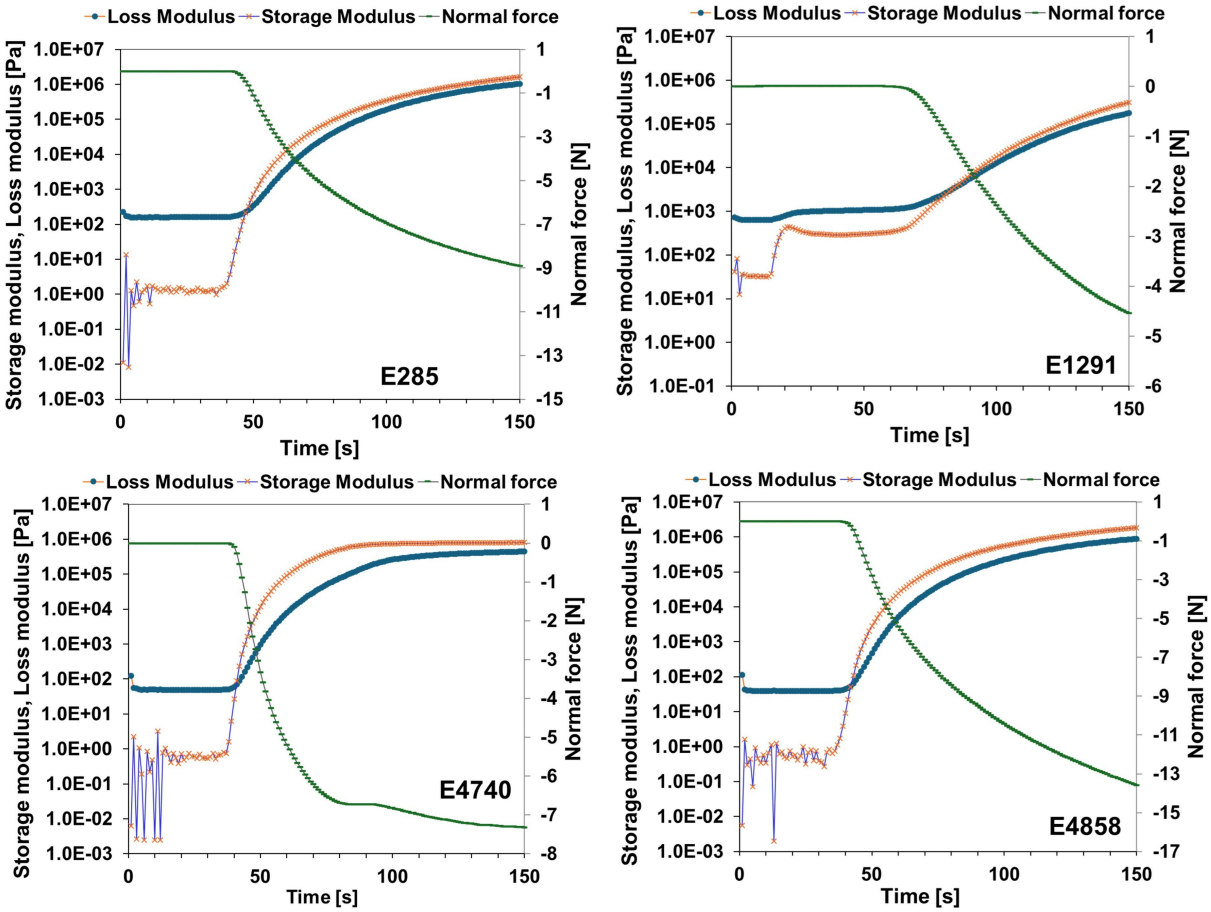


Figure 6. Determination of gel point by photorheology techniques for monomer-based compositions: EBECRYL 285 (E285), EBECRYL 1291 (E1291), EBECRYL 4740 (E4740), EBECRYL 4858 (E4858) in the presence of TPO (1% w/w) initiator. The samples were irradiated with a UV-LED with maximum emission at 365 nm and light intensity of 30 mW/cm$^2$.

Table 3. A summary of the times for the tested compositions (EBECRYL 285 (E285), EBECRYL 1291 (E1291), EBECRYL 4740 (E4740), EBECRYL 4858 (E4858) in the presence of the initiator TPO (1% by weight) ) to reach gelation points using the photorheology technique after LED irradiation with maximum emission at 365 nm (30 mW/cm$^2$).

| Sample name | Time to reach gelling point [s] | Polymerization shrinkage [%] |
|---|---|---|
| E285 | 47 | 0.30 |
| E1291 | 82 | 0.90 |
| E4740 | 41 | 0.50 |
| E4858 | 42 | 1.50 |

these resins in the 3D printing process in aqueous electrolyte environments by extruding the resin through appropriate nozzles and subsequently curing it with UV light. These resins are based on acrylate and acrylate-urethane monomers with a viscosity of around 20 000 Pa·s, combined with diphenyl(2,4,6-trimethylbenzoyl)phosphine oxide photoinitiator (TPO). These findings are highly relevant for the application of 3D printing with photocurable resins in multi-material 3D printers. Moreover, the study demonstrated the influence of the aqueous environment on the overall monomer conversion rate and the induction time of photopolymerization. The paper also proposes an explanation for the phenomena influencing the variation in photopolymerization induction times across different environments, such as oxygen and copper ion inhibition.

The literature includes studies on photopolymerization reactions that are thematically similar but focus on different applications of the process than the 3D printing of photocurable resins in electroplating baths described in this paper. Furthermore, as indicated in a 2024 publication, the in situ 3D printing technique with photocurable resins has not yet been tested for printing in an underwater environment (Korniejenko et al., 2024). The literature includes studies on topics such as the photopolymerization of methacrylic acid-based hydrogels in water (He et al., 2006), near-infrared light-induced radical polymerization in water (Neidinger et al., 2022) and novel water-soluble photoinitiators for acrylic photopolymerization (Kojima et al., 1998).

Based on the conducted studies, it was found that the aqueous electrolyte solution environment negatively impacts the photopolymerization process by reducing the conversion value of the monomer functional groups and increasing the polymerization induction time, consequently prolonging the curing time of the resin layer. The curing time of a single layer of photocurable resin strongly depends on the environment in which the resin layer is located due to the varying solubility of atmospheric oxygen and the presence of certain ions such as copper (II) ions, which inhibits the photoinitiation stage of polymerization by quenching free radicals in the surrounding environment and chain termination. According to kinetic studies using FPT, the type of environment does not affect the initial polymerization rate. However, Raman spectroscopy studies have shown that the attenuation of UV radiation through partial scattering and absorption in aqueous solutions reduces the conversion degree of the functional groups of the monomers used. When conducting photopolymerization in aqueous environments, to ensure a satisfactory photopolymerization rate and consequently a desired 3D printing speed, it is recommended to use strong UV light sources.

It was also shown that the polymerization shrinkage of the analyzed compositions does not reach high values. The highest shrinkage is 1.5% for the E4858 composition. So it can be assumed that the impact of polymerization shrinkage of the analyzed compositions on the formation of structural defects in 3D printed parts using analyzed resins is negligibly small.

In general, it can be concluded that the selected resins based on acrylate and acrylate-urethane monomers from the EBECRYL series with a viscosity on the level of 20 000 Pa·s, combined with the photoinitiator TPO, exhibit suitable rheological properties for maintaining coherence in an aqueous environment and satisfactory photoinitiation efficiency to be used for 3D printing in aqueous electrolyte solutions, such as electroplating baths used for metal electrodeposition. Therefore, it can be hypothesized that such resins could potentially serve as a material for 3D printing polymer parts in hybrid metal-polymer technology, utilizing coupled electrodeposition and photopolymerization processes.

Further stages of work in this area will involve application tests of these resins for 3D printing in an electroplating bath environment. Many technical aspects still require optimization in this area, such as the selection of UV light intensity and the distance of the UV source from the solution layer in such 3D printing devices. This issue thus represents a highly interesting research area with a highly interdisciplinary nature, encompassing both the further optimization of the composition of such resins and the design and construction of specialized 3D printing equipment for use with these resins in an aqueous environment.

## Acknowledgments

*The research work was conducted as part of the LIDER XII project (agreement no. LIDER/51/0270/L-12/20/NCBR/2021) titled „Multi-material 3D printer dedicated to production of solid metal and galvanic alloys parts, as well as metal-polymer hybrid elements using developed coupled technology of metal electrodeposition and photopolymerization of polymer resins" funded by the National Centre for Research and Development.*

## SYMBOLS

| | |
|---|---|
| *UV-Vis* | ultraviolet and visible light spectrum |
| *UV-LED* | Ultraviolet Light-Emitting Diode |
| *IR* | infrared light |
| $t_{ind}$ | induction time |
| $(dR/dt)_0$ | initial polymerization rate |
| *R* | fluorescence intensity ratio |
| *TPO* | Diphenyl(2,4,6-trimethylbenzoyl)phosphine oxide |
| *Coumarin 102* | 2,3,6,7-Tetrahydro-9-methyl-1*H*,5*H*-quinolizino (9,1-*gh*)coumarin |
| *FPT* | Fluorescence Probe Technology |
| *SLA* | Stereolitography |
| *DLP* | Digital Light Processing |
| *SLS* | Selective Laser Scattering |
| *EBM* | Electron Beam Melting |
| *EBAM* | Electron Beam Additive Manufacturing |
| *LMD* | Laser Material Deposition |
| *SLM* | Selective Laser Melting |
| *FDM* | Fused Deposition Modeling |
| *CLIP* | Continuous Liquid Interface Production |

## REFERENCES


Abramov L.I., Zilberman Y.N., Ivanova V.I., 1989. Effect of copper and iron salts on the radical polymerization of acrylamide in water. *Polym. Sci. U.S.S.R.*, 31, 1573–1578. DOI: 10.1016/0032-3950(89)90501-7.

Ahn D., Stevens L.M., Zhou K., Page Z.A., 2020. Rapid high-resolution visible light 3D printing. *ACS Cent. Sci.*, 6, 1555–1563. DOI: 10.1021/acscentsci.0c00929.

Ambrosi A., Webster R.D., Pumera M., 2020. Electrochemically driven multi-material 3D-printing. *Appl. Mater. Today,* 18, 100530. DOI: 10.1016/j.apmt.2019.100530.

Asif M., Lee J.H., Lin-Yip M.J., Chiang S., Levaslot A., Giffney T., Ramezani M., Aw K.C., 2018. A new photopolymer extrusion 5-axis 3D printer. *Addit. Manuf.*, 23, 355–361. DOI: 10.1016/j.addma.2018.08.026.

Asif M., Ramezani M., Sun X., Xu X., Giffney T., Aw K.C., 2017. A new 3D printing technique using extrusion of photopolymer. *Twenty-fifth International Conference on Process and Fabrication of Advanced Materials (PFAM-XXV)*. 22-25 January 2017, Auckland,New Zealand.

Bagheri A., Jin J., 2019. Photopolymerization in 3D printing. *ACS Appl. Polym. Mater.*, 1, 593–611. DOI: 10.1021/acsapm.8b00165.

Chen X., Liu X., Childs P., Brandon N., Wu B., 2017. A low cost desktop electrochemical metal 3D printer. *Adv. Mater. Technol.*, 2, 1700148. DOI: 10.1002/admt.201700148.

de Oliveira D.C.R.S., Rocha M.G., Correa I.C., Correr A.B., Ferracane J.L., Sinhoreti M.A.C., 2016. The effect of combining photoinitiator systems on the color and curing profile of resin-based composites. *Dent. Mater.*, 32, 1209–1217. DOI: 10.1016/j.dental.2016.06.010.

Duty C., Ajinjeru C., Kishore V., Compton B., Hmeidat N., Chen X., Liu P., Hassen A.A., Lindahl J., Kunc V., 2018. What makes a material printable? A viscoelastic model for extrusion-based 3D printing of polymers. *J. Manuf. Processes*, 35, 526–537. DOI: 10.1016/j.jmapro.2018.08.008.

Gibson I., Rosen D.W., Stucker B., 2010. *Additive manufacturing technologies. Rapid prototyping to direct digital manufacturing*. Springer New York, NY. DOI: 10.1007/978-1-4419-1120-9.

He H., Li L., Lee L.J., 2006. Photopolymerization and structure formation of methacrylic acid based hydrogels in water/ethanol mixture. *Polymer,* 47, 1612–1619. DOI: 10.1016/j.polymer.2006.01.014.

Huang B., Zhou Y., Wei L., Hu R., Zhang X., Coates P., Sefat F., Zhang W., Lu C., 2022. Visible light 3D printing of high-resolution superelastic microlattices of poly(ethylene glycol) diacrylate/graphene oxide nanocomposites via continuous liquid interface production. *Ind. Eng. Chem. Res.*, 61, 13052–13062. DOI: 10.1021/acs.iecr.2c01696.

Jandyal A., Chaturvedi I., Wazir I., Raina A., Haq M.I.U., 2022. 3D printing – a review of processes, materials and applications in industry 4.0. S*ustainable Oper. Comput.*, 3, 33–42. DOI: 10.1016/j.susoc.2021.09.004.

Kamińska I., Ortyl J., Popielarz R., 2015. Applicability of quinolizino-coumarins for monitoring free radical photopolymerization by fluorescence spectroscopy. *Polym. Test.*, 42, 99–107. DOI: 10.1016/j.polymertesting.2014.12.013.

Kamińska I., Ortyl J., Popielarz R., 2016. Mechanism of interaction of coumarin-based fluorescent molecular probes with polymerizing medium during free radical polymerization of a monomer. *Polym. Test.*, 55, 310–317. DOI: 10.1016/j.polymertesting.2016.09.013.

Khadilkar A., Wang J., Rai R., 2019. Deep learning–based stress prediction for bottom-up SLA 3D printing process. *Int. J. Adv. Manuf. Technol.*, 102, 2555–2569. DOI: 10.1007/s00170-019-03363-4.

Kojima K., Ito M., Morishita H., Hayashi N., 1998. A novel water-soluble photoinitiator for the acrylic photopolymerization type resist system. *Chem. Mater.*, 10, 3429–3433. DOI: 10.1021/cm9801688.

Korniejenko K., Gądek S., Dynowski P., Tran D.H., Rudziewicz M., Pose S., Grab T., 2024. Additive manufacturing in underwater applications. *Appl. Sci.*, 14, 1346. DOI: 10.3390/app14041346.

Kowsari K., Zhang B., Panjwani S., Chen Z., Hingorani H., Akbari S., Fang N.X., Ge Q., 2018. Photopolymer formulation to minimize feature size, surface roughness, and stair-stepping in digital light processing-based three-dimensional printing. *Addit. Manuf.*, 24, 627–638. DOI: 10.1016/j.addma.2018.10.037.

Lee J.-Y., An J., Chua C.K., 2017. Fundamentals and applications of 3D printing for novel materials. *Appl. Mater. Today*, 7, 120–133. DOI: 10.1016/j.apmt.2017.02.004.

Leprince J.G., Hadis M., Shortall A.C., Ferracane J.L., Devaux J., Leloup G., Palin W.M., 2011. Photoinitiator type and applicability of exposure reciprocity law in filled and unfilled photoactive resins. *Dent. Mater.*, 27, 157–164. DOI: 10.1016/j.dental.2010.09.011.

Meenakshisundaram V., Feller K., Chartrain N., Long T., Williams C., 2024. Characterizing photopolymer resins for high-temperature vat photopolymerization. *Prog. Addit. Manuf.*, 9, 2061–2071. DOI: 10.1007/s40964-023-00562-0.

Neidinger P., Davis J., Voll D., Jaatinen E.A., Walden S.L., Unterreiner A.N., Barner-Kowollik C., 2022. Near infrared light induced radical polymerization in water. *Angew. Chem. Int. Ed.*, 61, e202209177. DOI: 10.1002/anie.202209177.

Ngo T.D., Kashani A., Imbalzano G., Nguyen K.T.Q., Hui D., 2018. Additive manufacturing (3D printing): a review of materials, methods, applications and challenges. *Composites, Part B: Eng.*, 143, 172–196. DOI: 10.1016/j.compositesb.2018.02.012.

Olsen T.L., Tomlin B., 2019. Industry 4.0: opportunities and challenges for operations management. *Manuf. Serv. Oper. Manage.*, 22, 113–122. DOI: 10.1287/msom.2019.0796.

Ortyl J., Galek M., Milart P., Popielarz R., 2012. Aminophthalimide probes for monitoring of cationic photopolymerization by fluorescence probe technology and their effect on the polymerization kinetics. *Polym. Test.*, 31, 466–473. DOI: 10.1016/j.polymertesting.2012.01.008.

Pagac M., Hajnys J., Ma Q.-P., Jancar L., Jansa J., Stefek P., Mesicek J., 2021. A review of vat photopolymerization technology: Materials, applications, challenges, and future trends of 3d printing. *Polymers*, 13, 598. DOI: 10.3390/polym13040598.

Peruzzini M., Grandi F., Pellicciari M., 2020. Exploring the potential of Operator 4.0 interface and monitoring. *Comput. Ind. Eng.*, 139, 105600. DOI: 10.1016/j.cie.2018.12.047.

Praveena B.A., Lokesh N., Abdulrajak B., Santhosh N., Praveena B.L., Vignesh R., 2022. A comprehensive review of emerging additive manufacturing (3D printing technology): methods, materials, applications, challenges, trends and future potential. *Mater. Today*, 52, 1309–1313. DOI: 10.1016/j.matpr.2021.11.059.

Quan H., Zhang T., Xu H., Luo S., Nie J., Zhu X., 2020. Photocuring 3D printing technique and its challenges. *Bioact. Mater.*, 5, 110–115. DOI: 10.1016/j.bioactmat.2019.12.003.

Randhawa A., Dutta S.D., Ganguly K., Patel D.K., Patil T.V., Lim K.-T., 2023. Recent advances in 3D printing of photocurable polymers: types, mechanism, and tissue engineering application. *Macromol. Biosci.*, 23, 2200278. DOI: 10.1002/mabi.202200278.

Rau D.A., Forgiarini M., Williams C.B., 2021. Hybridizing Direct Ink Write and mask-projection Vat Photopolymerization to enable additive manufacturing of high viscosity photopolymer resins. *Addit. Manuf.*, 42, 101996. DOI: 10.1016/j.addma.2021.101996.

Sawicz-Kryniger K., Niezgoda P., Stalmach P., Starzak K., Wysocka A., Świergosz T., Popielarz R., 2022. Performance of FPT, FTIR and DSC methods in cure monitoring of epoxy resins. *Eur. Polym. J.*, 162, 110933. DOI: 10.1016/j.eurpolymj.2021.110933.

Shahrubudin N., Lee T.C., Ramlan R., 2019. An overview on 3D printing technology: technological, materials, and applications. *Procedia Manuf.*, 35, 1286–1296. DOI: 10.1016/j.promfg.2019.06.089.

Simič R., Mandal J., Zhang K., Spencer N.D., 2021. Oxygen inhibition of free-radical *polymerization is the dominant mechanism behind the "mold effect" on hydrogels. Soft Matter,* 17, 6394–6403. DOI: 10.1039/D1SM00395J.

Szymaszek P., Tomal W., Świergosz T., Kamińska-Borek I., Popielarz R., Ortyl J., 2023. Review of quantitative and qualitative methods for monitoring photopolymerization reactions. *Polym. Chem.*, 14, 1690–1717. DOI: 10.1039/d2py01538b.

Topa-Skwarczyńska M., Świeży A., Krok D., Starzak K., Niezgoda P., Oksiuta B., Wałczyk W., Ortyl J., 2022. Novel formulations containing fluorescent sensors to improve the resolution of 3D prints. *Int. J. Mol. Sci.*, 23, 10470. DOI: 10.3390/ijms231810470.

Yakout M., Elbestawi M.A., Veldhuis S.C., 2018. A review of metal additive manufacturing technologies. *Solid State Phenom.*, 278, 1–14. DOI: 10.4028/www.scientific.net/SSP.278.1.

Yang L., Hsu K., Baughman B., Godfrey D., Medina F., Menon M., Wiener S., 2017. Electron beam technology. In: *Additive manufacturing of metals: The technology, materials, design and production*. Springer Series in Advanced Manufacturing. Springer, Cham., 63–79. DOI: 10.1007/978-3-319-55128-9_4.

Zheng S., Zlatin M., Selvaganapathy P.R., Brook M.A., 2018. Multiple modulus silicone elastomers using 3D extrusion printing of low viscosity inks. *Addit. Manuf.,* 24, 86–92. DOI: 10.1016/j.addma.2018.09.011.